**Supporting Information**

# Defect-rich UiO-66@g-$C_3N_4$/Ni frameworks as efficient water splitting photocatalyst

Aparna Jamma[a, b], Bhavya Jaksani,[a, b] Chandra Shobha Vennapoosa[a, b], Spandana Gonuguntla[a, b], Saddam Sk[a, b], Mohsen Ahmadipour,[c] B. Moses Abraham [d], Indranil Mondal[e], Ujjwal Pal*[a, b]

[a]Department of Energy & Environmental Engineering, CSIR Indian Institute of Chemical Technology, Tarnaka, Hyderabad, Telangana, 500007, India

[b]Academy of Scientific and Innovative Research (AcSIR), Ghaziabad - 201002, India

[c]Institute of Power Engineering, Universiti Tenaga Nasional, Kajang, 43000, Selangor, Malaysia.

[d]Department of Chemical Engineering, Indian Institute of Technology Kanpur, Kanpur, 208016, India

[e]School of Chemistry, Indian Institute of Science Education and Research Thiruvananthapuram, Vithura, Thiruvananthapuram 695551, India

## Table of content

## 1. S1. Experimental Section:

### S1.1 Materials & Reagents

Zirconium chloride ($ZrCl_4$, Merck), Terephthalic Acid ($H_2BDC$, Avra Chemicals), N, N-Dimethylformamide (DMF, Finar Chemicals), Glacial Acetic Acid ($CH_3COOH$, Merck), Triethylamine ($C_6H_{15}N$, Sigma-Aldrich), Melamine ($C_3H_6N_6$, Sigma-Aldrich), Nickel Nitrate ($Ni(NO_3)_2.6H_2O$, Sigma Aldrich), Deionized water (18.2 mS conductivity). All chemicals were used without further purification.

### S1.2 Preparation of integrated photo-catalyst

**Synthesis of UiO-66**

UiO-66 photocatalyst was synthesized via solvothermal method as reported earlier.[1]0.25 g (1.5 mmol) of Terephthalic acid and 150 µL of triethylamine was dissolved in 25 mL of DMF.

Separately, 0.35 g (1.5 mmol) of $ZrCl_4$, and 6.9 mL of acetic acid were mixed with 25 mL of DMF. The solutions of Terephthalic acid and $ZrCl_4$ were combined and stirred for 30 min at R.T. The combined solution was transferred into 100ml Teflon coated autoclave, capped and placed in oven at 150$^o$C for 24h.After cooling the reaction mixture to room temperature, the sample was collected through centrifugation. The sample was rinsed several times with DMF and methanol to remove unreacted metal salts/organic moieties. Finally, UiO-66 was dried at 60$^o$C under vacuum overnight.

$$6H_2BDC + 6ZrCl_4 \xrightarrow[150^oC/24h]{DMF/TEA/CH_3COOH} Zr_6O_4(OH)_4(BDC)_6 + 24HCl$$

**Synthesis of g-$C_3N_4$**

5 g of melamine ($C_3H_6N_6$) was weighed and grounded with the help of mortar and pestle, for 10 min to maintain saturation and equilibrium. The finely ground mixture was then calcined at 500 $^o$C with a rate of 10$^o$C/min and held for a period of 2 h. An additional step of 5$^o$C/min up to500 $^o$C, with a hold of 2 h, resulted in the production of g-$C_3N_4$.[2]

**Defect formation experiments:**

**Synthesis of Defect UiO-66**

40mg $AgNO_3$, 40 mg $K_2S_2O_8$ and 300mg UiO-66 powder were dissolved into 40ml Acetonitrile. The mixture was sonicated for 10min & the resultant mixed solution was placed in a preheated oil bath at 120$^o$C for 60min. When the reaction was finished, immediately move into ice water for quenching and to prevent further decarboxylation etching. After cooling, the decarboxylated UiO-66 was collected by centrifugation and washed with Deionized water for 3times and finally dried at 70$^o$C overnight.[3]

**Synthesis of UiO-66@g-$C_3N_4$and UiO-66-D@g-$C_3N_4$ hybrid photocatalyst**

The synthesis method of UiO-66@g-$C_3N_4$ was mentioned in previous literature. The UiO-66@g-$C_3N_4$ hybrids (U6g- *x, x* = 10, 20, 30, 40 and 50) were fabricated by thermal treating the mixture of g-$C_3N_4$ and UiO-66 octahedrons. In a typical procedure, a certain amount of UiO-66 octahedrons and g-$C_3N_4$ powders were mixed in the mortar and ground for30 min using a pestle. The ground mixture was then thermal treated at 350°C for 2 h in Ar atmosphere in a tube furnace

to produce the UiO-66@g-$C_3N_4$ heterojunctions. Similarly, UiO-66-D@g-$C_3N_4$is prepared also using the above same procedure to replace UiO-66.

**Synthesis of UiO-66@g-$C_3N_4$/Ni and UiO-66-D@g-$C_3N_4$/Ni**

UiO-66@g-$C_3N_4$/Ni was synthesized by a post synthetic metalation method. As prepared UiO-66@g-$C_3N_4$ (0.1 g) was transferred into round bottom flask, which contained10 mL of N, N′ Dimethyl formamide. After sonication for1 min, a certain amount of Ni $(NO_3)_2.6H_2O$ (0.1, 0.5, 1.0, 2.0, 2.5 wt%) was added into the suspension solution. Then, the flask was sealed, heated, and maintained at 90°C for 24 h. The slight brown solids were collected and washed 2 times with N, N′-dimethylformamide and methanol, respectively. The final products of UiO-66@g-$C_3N_4$/Ni were finally dried at 60°Cfor 24 h in the oven and named UiO-66@g-$C_3N_4$/Ni*x* (*x*: .1, 0.5, 1.0, 2.0, 2.5). Similarly, UiO-66-D@g-$C_3N_4$/Ni was prepared using the above methodology.

**Synthetic methodology:**

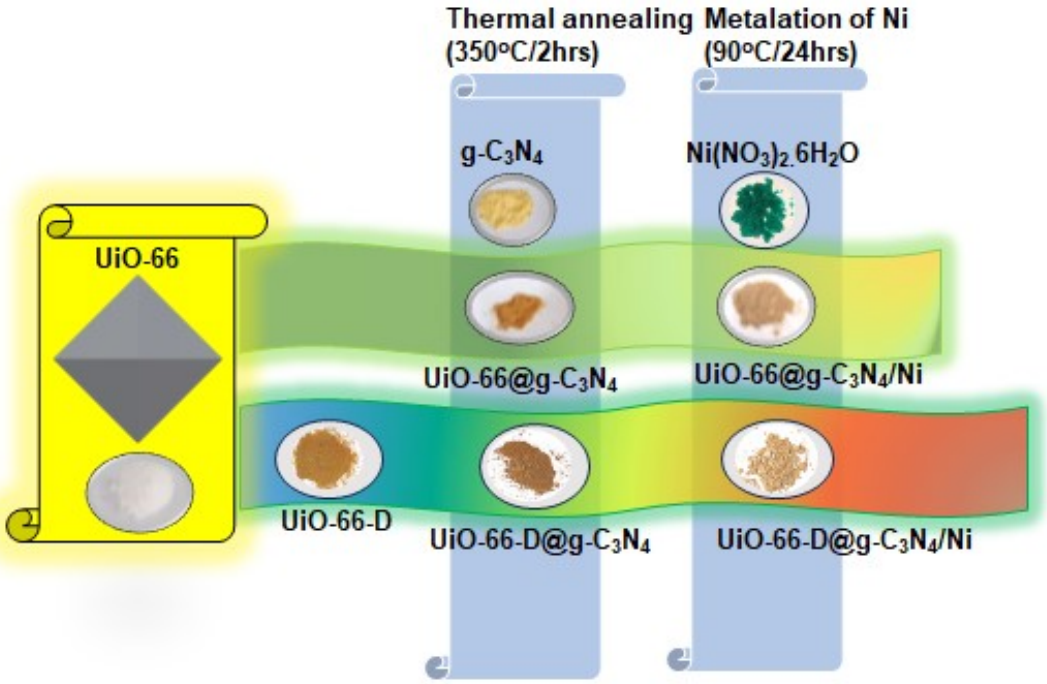


**Scheme S1:** The fabrication process of the UiO-66@g-$C_3N_4$/Ni & UiO-66-D@g-$C_3N_4$/Ni

**S1.2 Characterization**

The structural phase analysis of the as-synthesized photocatalysts was performed by using Powder X-ray diffraction patterns (XRD) on a Bruker AXS diffractometer (D8 advance) at a generator voltage of 40 kV and current of 30 mA using Cu-Kα1 irradiation (λ = 1.5406 Å). The sample was scanned in the range of 2θ = 10-80° with a scan rate of 1 s/step. X-ray photoelectron spectroscopy (XPS) was performed via a Kratos (axis 165) analytical instrument with Mg Kα irradiation. About 10-9 Torr pressure was maintained in the spectrometer. The structural morphology of the photocatalysts was examined by using MIRA3 FEG-SEM (TESCAN) Scanning electron microscopy (SEM) at an accelerating voltage of 5 kV. Transmission electron microscopy (TEM) image of the representative photocatalysts was obtained by using a JEOL 2010EX TEM instrument equipped with the high-resolution style objective-lens pole piece at an acceleration voltage of 200 kV fitted with a CCD camera. $N_2$ adsorption-desorption isotherms of the photocatalysts were obtained on a Quanta chrome Nova 2200e gas adsorption analyzer at 77 K. The optical properties were characterized by using UV-Vis diffuse reflectance spectroscopy (DRS) Perkin Elmer Lambda 750 instrument using $BaSO_4$ as a reference. The sample has been placed in the sample holder for the measurement and the light is allowed to pass through the sample which leads to the absorption of the light and the light transmitted by the sample has been recorded. The Photoluminescence (PL) spectra were recorded using a Fluorolog-3 spectrofluorometer ($Sp_{ex}$ model, JobinYvon) at their respective excitation ($\lambda_{ex}$) wavelength. Fluorescence Lifetime decay measurements were carried out by using time-correlated single-photon counting (TCSPC) setup (Fluorolog-3 Triple Illuminator, IBH Horiba Jobin Yvon). Briefly, the samples were excited at 380 nm, and the emission was observed at 434 nm.

**S1.3 Computational details:**

Utilizing projector augmented wave (PAW) pseudopotentials[4], we performed plane-wave density functional theory (DFT) calculations using Vienna ab initio simulation package (VASP) code[5] to describe the interactions between the valence electrons and the core ions. The widely employed Perdew-Burke-Ernzerhof (PBE) functional [6], which belongs to the generalized gradient approximation (GGA) schemes was incorporated to account for the electron exchange correlation. In order to obtain ground-state atomic geometries, the conjugate-gradient algorithm is used to minimize the Hellman-Feynman forces on each ion to < 0.02 eV/Å, while Kohn-Sham orbitals were expanded through a plane wave cutoff energy of 520 eV. We ensured sufficient accuracy by

converging the self-consistent electronic cycles up to $10^{-5}$ eV. For the structural relaxation, the Monkhorst-Pack scheme [7] was adopted, using a K-point mesh of 3 × 3 × 1 for efficient Brillouin Zone integration. To account for van der Waals (vdW) interactions, Grimme's DFT-D3 method [8] is utilized, considering the long-range interactions. The defect UiO-66 structure (UiO-66-D) is modeled by eliminating organic linkers from the cluster, resulting in vacancies on neighboring $Zr^{4+}$ ions (see Figure S2). Cleaving the bulk model resulted in obtaining the g-$C_3N_4$ monolayer and subsequently the UiO-66-D@g-$C_3N_4$ complex is generated with the optimized UiO-66-D positioned on top of the g-$C_3N_4$ layer, as shown in Figure 5d. When modeling the catalyst, a 15 Å vacuum is introduced along the z-direction to prevent interactions between adjacent slabs.

**S1.4 Photo-electrochemical studies**

The entire photo-electrochemical test was carried out in the electrochemical workstation. 0.25 M aqueous solution of $Na_2SO_4$ was used as an electrolyte for all experiments. Pt wire and calomel electrodes were used as counter and reference electrodes. The preparation of the working electrode is carried out using 20 µL of suspension (5 mg in 1mL ethanol) on ITO coated glass surface with a specific area of 2 $cm^2$. The light source is considered as a Photoelectrochemical measurement at room temperature were recorded on the CH Instruments Inc., USA, CHI6005E, Electrochemical Workstation with Potentiostat using a three-electrode system with a standard three-electrode system with the photocatalyst-coated ITO as the working electrode, Pt wire as the counter electrode, Ag/AgCl electrode as the reference electrode. The artificial solar simulator of AM 1G illuminator (100 mW $cm^{-2}$) was used as the light source during the measurement. The electrochemical cell was a conventional 7 three-electrode cell with a 3 mm thick Pyrex glass eyelet. A 0.25 M $Na_2SO_4$ solution was used as the electrolyte. **Electrode Preparation:** To prepare the photo electrode, 4 mg of each as-synthesized photocatalyst was dispersed into a suspension that contained 0.3 ml ethanol and 40 µmol Nafion by 30 min of ultrasonication. The as-prepared solution was dropped on the surface of Indium tin oxide (ITO) film of 2 × 2 $cm^2$ surface area to achieve uniform coverage and then dried in air at room temperature

**S1.5 Photocatalytic Hydrogen Production**

The photocatalytic $H_2$ production activity of the as-synthesized materials was evaluated with 20 mL of aqueous 10% (v/v) TEOA and Eosin Y (EY) photosensitizer mixture at neutral pH under simulated light irradiation of $\lambda \geq 420$ nm. Photocatalytic experiments were conducted in a 90ml

quartz reactor. In a typical photocatalytic experiment, 10 mg of catalyst was suspended in 20ml water and 2 ml triethanolamine (10vol%) in which neutral pH is maintained using 1M HCl. 1.29 mg dye Eosin Y (EY) ($0.1\times10^{-3}$ M) is added by means of ultrasonication for about 10 min. The opening of the reactor was sealed with a silicone rubber septum. The degassing and insertion of the inert atmosphere ($N_2$) have been carried out for a period of 30 min through this portion of the reactor. Then the reactor is kept under a 420 W Xe arc lamp light irradiation (Newport Co., Ltd., USA and working at 400 W) with constant stirring. The evolved $H_2$ gas was analyzed at a periodic interval (every hour) using gas chromatography (Perkin Elmer Clarus 590 GC containing molecular Sieve/5 A˚ column) with a thermal conductivity detector using $N_2$ as a carrier gas. The AQY (%) and the values of the Number of incident photons ($N_{photons}$) were calculated using the following equations**:** $N_{photon} = \frac{P\lambda t}{hc}$

Here, P = power of light (0.19 J $s^{-1}$ $cm^{-2}$) over a specific area of 12.26 $cm^2$, λ = light wavelength (400 nm), t = irradiation time (4 h), h - Planck's constant ($6.626 \times 10^{-34}$ J s) and c = velocity of light ($3 \times 10^8$ m $s^{-1}$).

$$AQY\ \% = \frac{2 \times the\ no.\ of\ evolved\ H_2\ molecule}{the\ no.\ of\ incident\ photons\ (N_{photon})} \times\ 100$$

**Table S1:** Elemental composition of UiO-66, UiO-66@g-$C_3N_4$ and UiO-66@g-$C_3N_4$/Ni analyzed by EDX

| Catalyst | Atom (%) | | | | |
|---|---|---|---|---|---|
| | **C** | **O** | **Zr** | **Ni** | **N** |
| UiO-66 | 51.3 | 35.9 | 12.8 | - | - |
| UiO-66@g-$C_3N_4$ | 56.0 | 24.0 | 19.2 | - | 0.8 |
| UiO-66@g-$C_3N_4$/Ni | 46.6 | 25.7 | 21.6 | 2.5 | 3.6 |

**Table S2.** Physical Adsorption Performance Parameters

| Sample | $S_{BET}$ ($m^2/g$) | Pore volume ($cm^3/g$) | Average pore size (nm) |
|---|---|---|---|
| g-$C_3N_4$ | 394.20 | 2.14 | 2.17 |
| UiO-66 | 858.00 | 0.58 | 2.69 |
| UiO-66-D | 907.90 | 0.51 | 2.21 |
| UiO-66@Ni/g-$C_3N_4$ | 549.90 | 1.13 | 5.62 |
| UiO-66-D@Ni/g-$C_3N_4$ | 808.00 | 0.52 | 11.21 |

**Table S3. Comparative table of the average lifetime of the photocatalysts.**

| **Photocatalyst** | **$\tau_1$ (ns)** | **$\tau_2$ (ns)** | **$\tau_3$ (ns)** | **Average Lifetime (ns)** |
|---|---|---|---|---|
| UiO-66 | **2.67** | 8.56 | 2.74 | 1.62 |
| UiO-66-D | 1.23 | 3.84 | - | 1.82 |
| UiO-66@g-$C_3N_4$/Ni | 2.10 | 1.14 | 9.21 | 3.08 |

| | | | | |
|---|---|---|---|---|
| UiO-66-D@ g-$C_3N_4$/Ni | 1.16 | 5.06 | 3.71 | 3.70 |

**Table S4. Photocatalytic $H_2$ generation efficiency of the composites under visible light irradiation for 4 hrs**

| Sl. No | Photocatalysts | $H_2$ activity ($mmolg^{-1}h^{-1}$) TEOA | $H_2$ activity ($mmolg^{-1}h^{-1}$) TEOA/Eosin-Y | AQY (%) | AQY (%) |
|---|---|---|---|---|---|
| 1 | UiO-66 | 0.09 | 0.41 | 0.2 | 1 |
| 2 | g-$C_3N_4$ | 0.42 | 0.78 | 0.69 | 1.7 |
| 3 | UiO-66@g-$C_3N_4$ | 0.17 | 1.06 | 0.41 | 2.59 |
| 4 | UiO-66@g-$C_3N_4$/Ni (0.1%) | 0.19 | 1.08 | 0.31 | 1.7 |
| 5 | UiO-66@g-$C_3N_4$/Ni (0.5%) | 0.21 | 1.58 | 0.34 | 2.61 |
| 6 | UiO-6@g-$C_3N_4$/Ni (1.0%) | 0.23 | 1.66 | 0.38 | 2.72 |
| 7 | UiO-66@g-$C_3N_4$/Ni (2.0%) | 0.24 | 2.05 | 0.58 | 5.1 |
| 8 | UiO-66@g-$C_3N_4$/Ni (2.5%) | 0.22 | 1.28 | 0.36 | 2.11 |
| 9 | UiO-66@Ni (2.0%) | 0.13 | 0.56 | 0.24 | 0.92 |
| 10 | UiO-66-D | 0.11 | 0.65 | 0.26 | 1.4 |
| 11 | UiO-66-D@g-$C_3N_4$ | 0.21 | 1.37 | 0.51 | 3.3 |
| 12 | UiO-66-D@g-$C_3N_4$/Ni (0.1%) | 0.25 | 1.47 | 0.61 | 2.41 |
| 13 | UiO-66-D@g-$C_3N_4$/Ni (0.5%) | 0.26 | 2.09 | 0.63 | 3.45 |

| | | | | | |
|---|---|---|---|---|---|
| 14 | UiO-66-D@g-$C_3N_4$/Ni (1.0%) | 0.27 | 2.21 | 0.66 | 3.65 |
| 15 | UiO-66-D@g-$C_3N_4$/Ni (2.0%) | 0.29 | 2.62 | 0.71 | 6.41 |
| 16 | UiO-66-D@g-$C_3N_4$/Ni (2.5%) | 0.26 | 1.58 | 0.63 | 2.61 |
| 17 | UiO-66-D@Ni (2.0%) | 0.18 | 0.74 | 0.02 | 1.81 |

**Table S5. Comparative table of photocatalytic hydrogen evolution activity.**

| **Photocatalyst** | **Incorporated Component** | **Condition** | **SED** | **$H_2$ activity** mmol $g^{-1}$ $h^{-1}$ | **Ref.** |
|---|---|---|---|---|---|
| UiO-66-PANI-$Co_3O_4$ | Co | 450W λ =420nm | TEOA | 710 | 9 |
| Pt/UiO-66@g-$C_3N_4$ | Pt | 300W λ =420nm | L -ascorbic acid | 0.14 | 10 |
| D-UiO-66-$NH_2$/ZIS | - | 300W λ =420nm | $Na_2S$&$Na_2SO_3$ | 7.3 | 11 |
| UiO-66-$NH_2$/$MoS_2$ | $MoS_2$ | 300W λ =420nm | Methanol | 0.5 | 12 |
| Pt/UiO-66/CdS | Pt | 300W λ =420nm | L -ascorbic acid | 4.7 | 1 |

| | | | | | |
|---|---|---|---|---|---|
| UiO-66-$NH_2$/$Cd_{0.2}Zn_{0.8}S$ | - | 300W λ =420nm | $Na_2S$&$Na_2SO_3$ | 5.8 | 13 |
| UiO-66-$NH_2$/Graphene | Pt | 300W λ =420nm | TEOA | 41.4 | 14 |
| sg-CN | Ni | 300W λ =420nm | TEOA | 0.103 | 15 |

## 2. S2 Figures

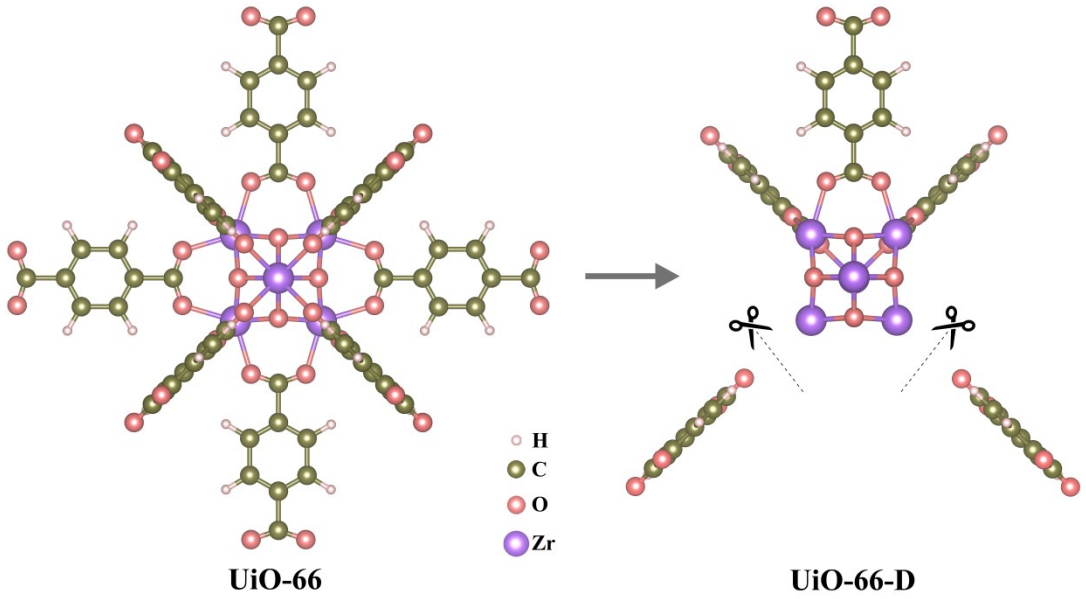


**Figure S1**. Schematic representation illustrating the formation of defect-induced UiO-66 (UiO-66-D) through eliminating organic linkers from the cluster, resulting in vacancies on neighboring $Zr_4^+$ ions.

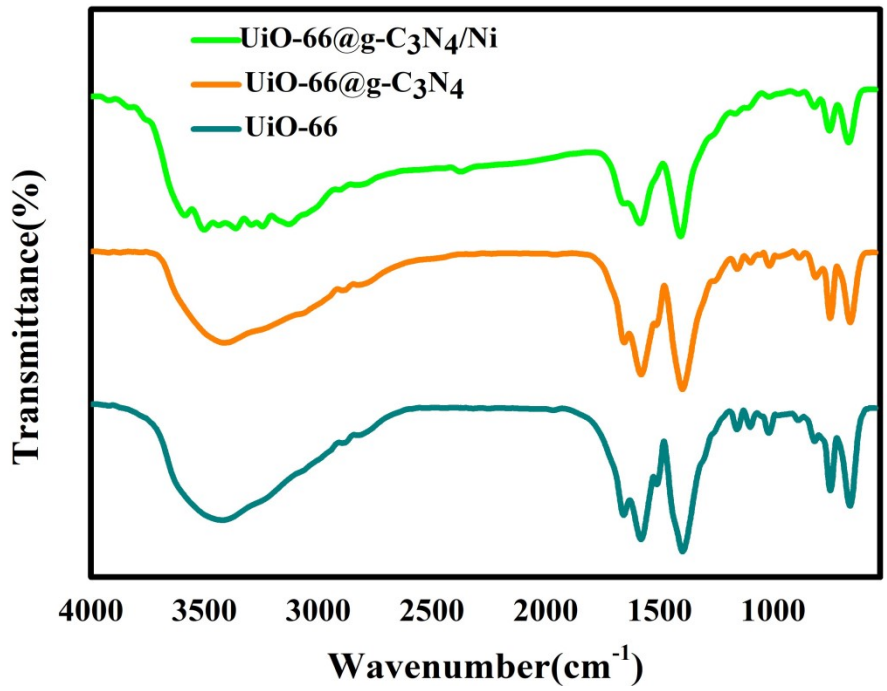


**Figure S2**. FTIR analysis of prepared UiO-66 variations.

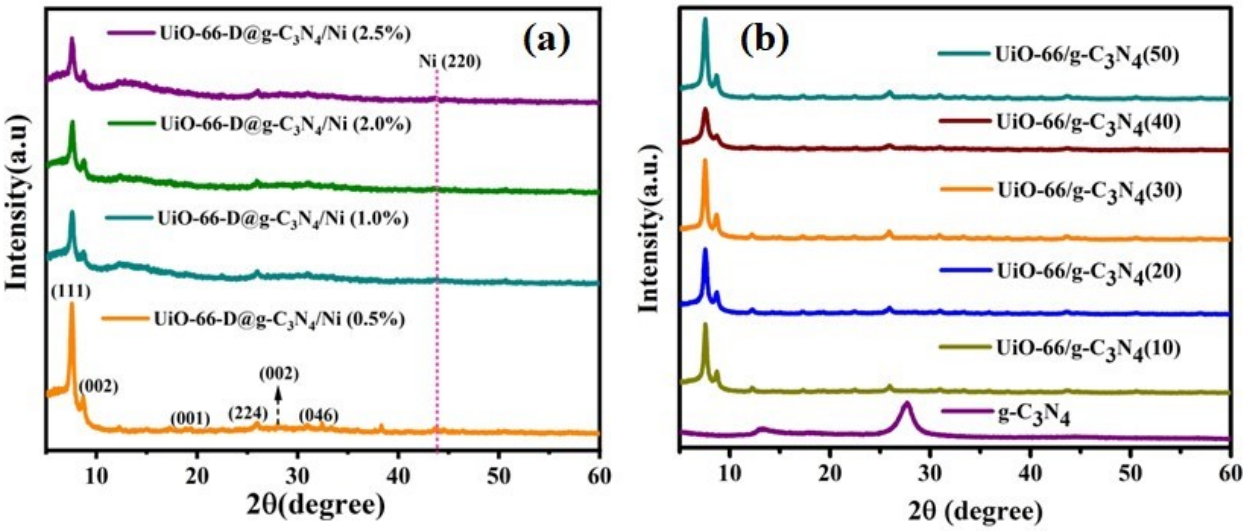


**Figure S3**. PXRD analysis of prepared UiO-66 variations

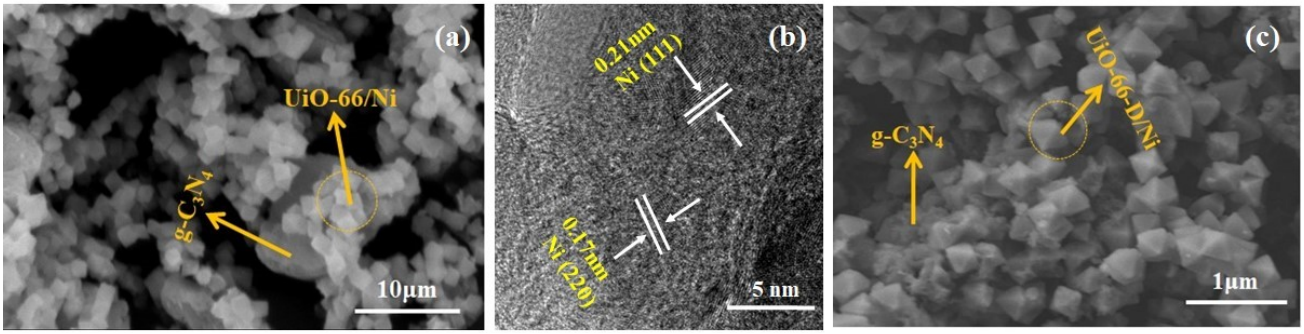


**Figure S4.** SEM image of (a) UiO-66@g-$C_3N_4$/Ni, (c) UiO-66-D@g-$C_3N_4$/Ni and (b) HRTEM for Ni NPs encapsulated in UiO-66-D@g-$C_3N_4$ composite.

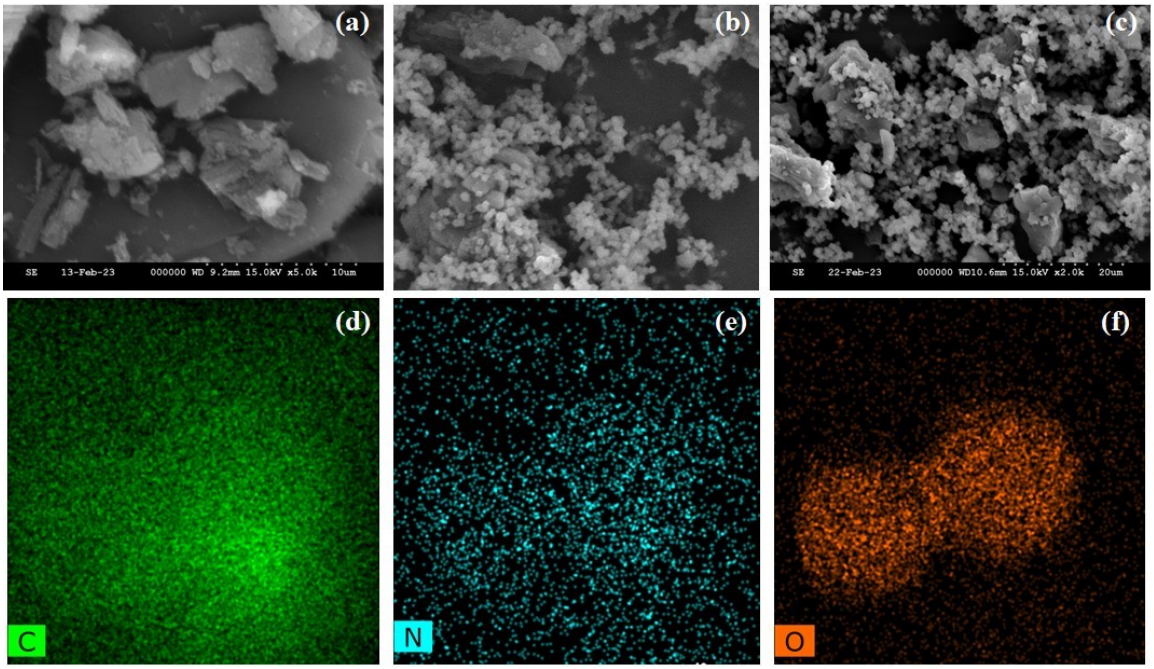


**Figure S5.** FESEM analysis of (a) g-$C_3N_4$ (b) UiO-66@g-$C_3N_4$ and (c) UiO-66-D@g-$C_3N_4$ photocatalysts, TEM Elemental analysis of (d) C, (e) N, (f) O.

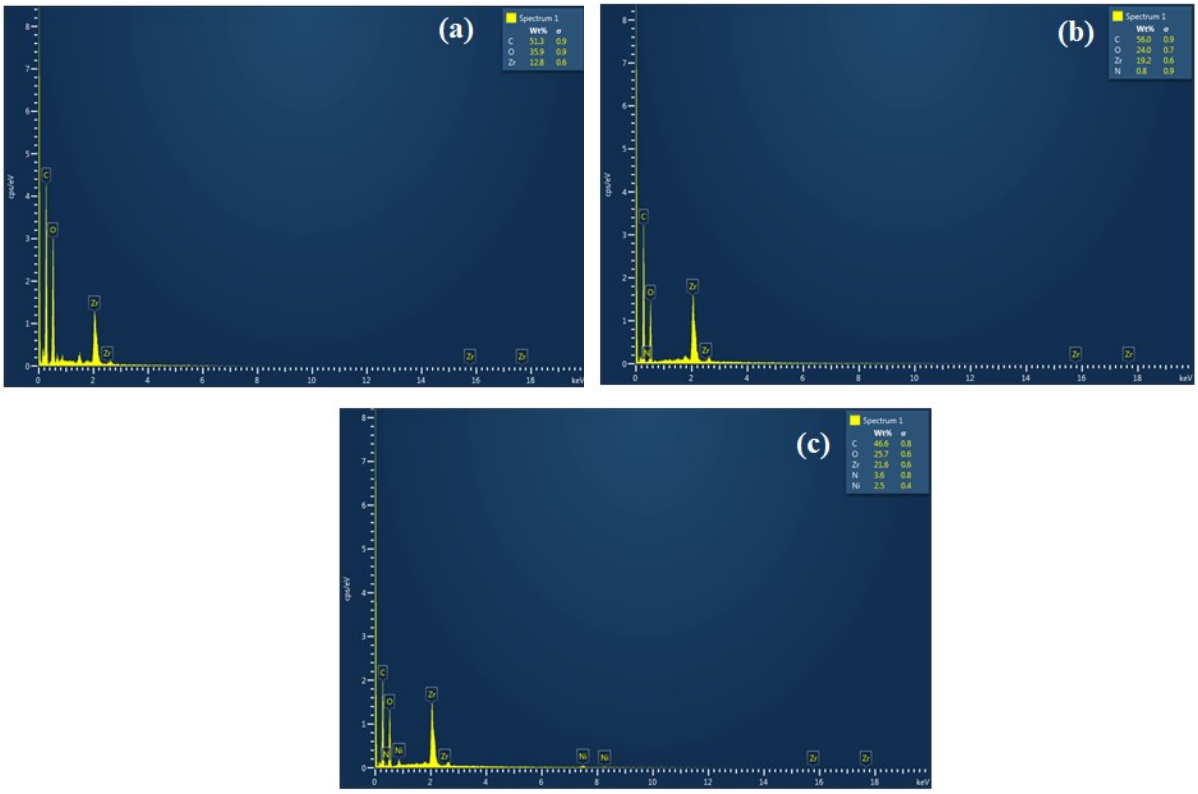


**Figure S6.** Energy-dispersive X-ray (EDX) spectra of (a) UiO-66, (b) UiO-66@g-$C_3N_4$ and (c) UiO-66@g-$C_3N_4$/Ni

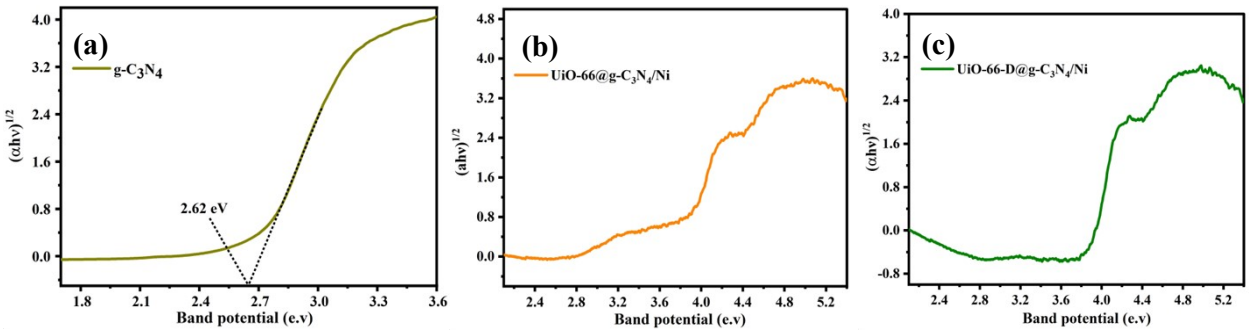


**Figure S7.** Band gap potentials (Tauc plots) of (a) g-$C_3N_4$, (b) UiO-66@g-$C_3N_4$/Ni, (c) UiO-66-D@g-$C_3N_4$/Ni

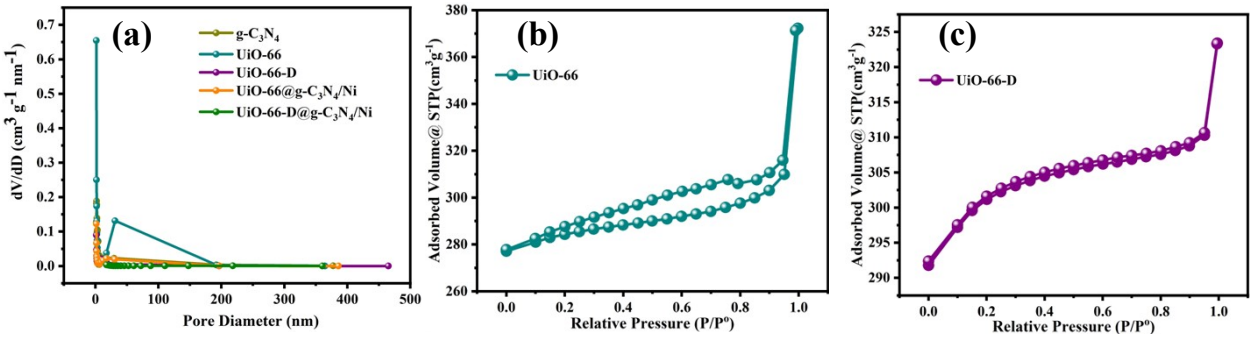


**Figure S8.** (a) Barrett- Joyner-Halenda (BJH) Pore size distribution curves of UiO-66 prepared photocatalysts, $N_2$ adsorption-desorption isotherm of (b) UiO-66, (c) UiO-66-D

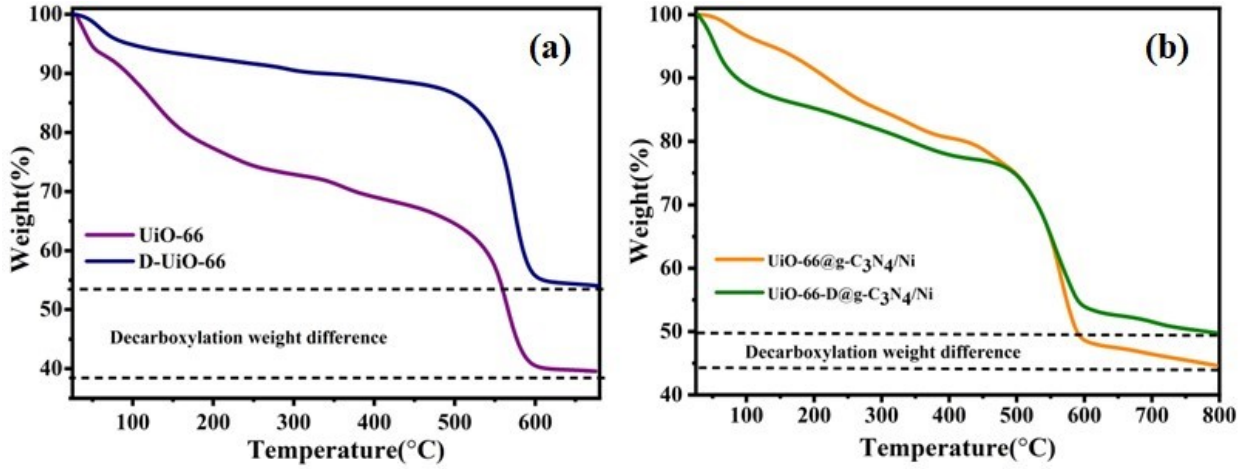


**Figure S9**. TGA analysis of (a) UiO-66 samples, (b) final composites.

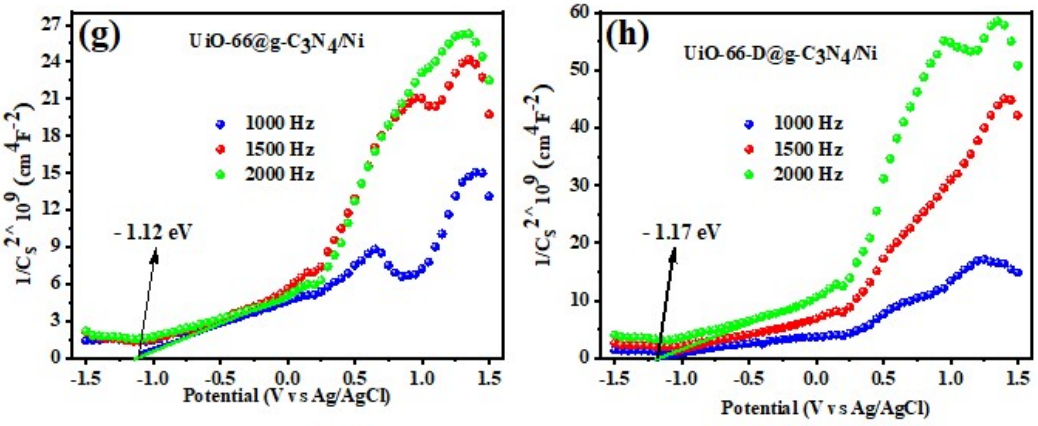


**Figure S10.** Mott-Schottky plots of as-synthesised photocatalysts.

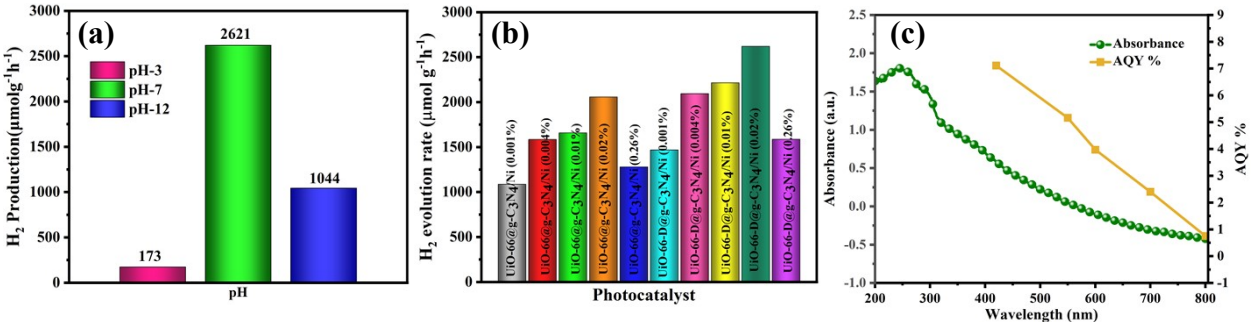


**Figure S11**. Histograms showing the rate of $H_2$ production (a) performed in different pH medium, (b) % Ni variation in defect and non-defect photocatalysts at neutral pH, (c) Comparison of DRS spectra and AQY values of UiO-66-D@g-$C_3N_4$/Ni under optimal photoreaction conditions and different monochromatic light irradiation.

**References**


1. Zhou, J-J.; Wang, R.; Liu, X-L.; Penga, F-M.; Li, C-H.; Teng, F.; Yuan, Y-P. In situ growth of CdS nanoparticles on UiO-66 metal-organic framework octahedrons for enhanced photocatalytic hydrogen production under visible light irradiation. Applied Surface Science. **2015**, 34, 6278–283.
2. Gonuguntla, S.; Sk, S.; Tiwari, A.; Mandal, H.; Lakavath, P-N.; Perupoga, V.; Pal, U. Regulating surface structures for efficient electron transfer across h-BN/$TiO_2$/g-$C_3N_4$ photocatalysts for remarkably enhanced hydrogen evolution. J Mater Sci: Mater Electron. **2021**, 32, 12191–12207.
3. Jeong, G-Y.; Singh, A.K.; Kim, M-G.; Gyak, K-W.; Ryu, U.; Choi, K.M.; Kim, D-P. Metal-organic framework patterns and membranes with heterogeneous pores for flow-assisted switchable separations. Nat Commun 9, **2018**, 3968-3977.
4. Blochl, P. E. Projector augmented-wave method. Phys. Rev. B: Condens. Matter Mater. Phys. **1994**, 50, 17953-17979.
5. Kresse, G.; Furthmüller. J. Efficient iterative schemes for ab initio total-energy calculations using a plane-wave basis set. *Phys. Rev. B*. **1996**, 54, 11169-11186.
6. Perdew, J. P.; Burke, K.; Ernzerhof. M.; Generalized Gradient Approximation Made Simple. Phys. Rev. Lett. **1996**, 77, 3865-3868.
7. Monkhort, H. J.; Pack. J. D. Special points for Brillouin-zone integrations. Phys. Rev. B: Solid State. **1976**, 13, 5188-5192.

8. Grimme, S.; Antony, J.; Ehrlich, S.; Krieg. H. A consistent and accurate ab initio parametrization of density functional dispersion correction (DFT-D) for the 94 elements H-Pu. J. Chem. Phys. **2010**, 132, 154104-154123.
9. Singh, A.K.; Gonuguntla, S.; Mahajan, B.; Pal, U. Noble metal-free integrated UiO-66-PANI-$Co_3O_4$ catalyst for visible-light-induced $H_2$ production. Chem. Commun. **2019**, 55, 14494-14497.
10. Wang, R.; Gu, L.; Zhou, J.; Liu, X.; Teng, F.; Li, C.; Shen, Y and Yuan, Y. Quasi-Polymeric Metal–Organic Framework UiO-66/g-$C_3N_4$ Heterojunctions for Enhanced Photocatalytic Hydrogen Evolution under Visible Light Irradiation. Adv. Mater. Interfaces **2015**, 2, 1500037-1500041.
11. Zhao, C.; Jiang, H.; Liang, Q.; Zhou, M.; Zhang, Y.; Li, Z.; Xu, S. $NH_2$-UiO-66 with heterogeneous pores assists zinc indium sulfide in accelerating the photocatalytic $H_2$ evolution under visible-light irradiation. Solar Energy. **2020**, 207, 599–608.
12. Subudhi, S.; Swain, G.; Tripathy, S.P.; Parida, K. UiO-66-$NH_2$ Metal−Organic Frameworks with Embedded $MoS_2$ Nanoflakes for Visible-Light-Mediated $H_2$ and $O_2$ Evolution. Inorg. Chem. **2020**, 59, 9824–9837.
13. Su, Y.; Zhang, Z.; Liu, H.; Wang, Y. $Cd_{0.2}Zn_{0.8}S$@UiO-66-$NH_2$ nanocomposites as efficient and stable visible-light-driven photocatalyst for $H_2$ evolution and $CO_2$reduction. Applied Catalysis B: Environmental. **2017**, 200, 448–457.
14. Wang, Y.; Yu, Y.; Li, R.; Liu, H.; Zhang, W.; Ling, L.; Duan, W.; Liu, B. Hydrogen production with ultrahigh efficiency under visible light by graphene well-wrapped UiO66-$NH_2$ octahedrons. J.Mater.Chem.A. **2017**, 5, 20136–20140.
15. Indra, A.; Menezes, P.W.; Kailasam, K.; Hollmann, D.; Schroder, M.; Thomas, A.; Bruckner, A.; Driess, M. Nickel as a co-catalyst for photocatalytic hydrogen evolution on graphitic-carbon nitride (sg-CN): what is the nature of the active species? Chem. Commun., **2016**, 52, 104 -107.